Hydrated Eutectic Electrolyte with Ligand-Oriented Solvation Shell to Boost the Stability of Zinc Battery

By Mingming Han, Jiwu Huang, Xuesong Xie, Tian Chen Li, Jiangtao Huang, Shuquan Liang, Jiang Zhou, and Hong Jin Fan**

M. Han, X. Xie, J. Huang, Prof. J. Huang, Prof. S. Liang, Prof. J. Zhou*

School of Materials Science and Engineering, Central South University, Changsha 410083, China

E-mail: zhou_jiang@csu.edu.cn

M. Han, Prof. H. J. Fan*

School of Physical and Mathematical Sciences, Nanyang Technological University, Singapore 637371, Singapore

E-mail: fanhj@ntu.edu.sg

T. C. Li

Pillar of Engineering Product Development, Singapore University of Technology and Design, 8 Somapah Road, Singapore 487372, Singapore.

ABSTRACT: Despite the substantial progress in cathode materials in the past few years, rechargeable zinc batteries (RZBs) are plagued by rapid performance degradation due to dendrite formation and notorious side reactions at the Zn anode side. Here, we propose an optimized hydrated eutectic electrolyte (HEE) system containing methylsulfonylmethane (MSM), zinc perchlorate and water, in which an organic ligand coordinated solvation shell of Zn ions with water molecules constituting the eutectic network. Compared to the common aqueous solutions, this HEE system is proven effective in promoting the smooth Zn deposition and plating/stripping reversibility as well as suppressing side reactions. The vanadium-based zinc batteries based on this new HEE exhibit exceptionally high-capacity retention (~100% retention even after 1600 cycles at a relatively small current density of 1000 mA g^{-1}). This study offers a new type of electrolyte for RZBs and a deep understanding of the effect of Zn^{2+} solvent sheath structure to the cycle reversibility.

1. Introduction

Aqueous Zinc batteries are believed to be a highly potent technology for grid-scale energy storage applications because of their appealing advantages over the conventional nonaqueous Li-based batteries in terms of high power and safety, environment friendless, and low cost.[1] Indeed, there has been tremendous progress in the past few years in the RZB cathode materials and intercalation mechanisms.[2] In the past few years, increasing attentions are being paid to the Zn anode side to mitigate the pitfalls of side reactions and dendrite growth.[3] The suboptimal cycling stability resulting from uncontrolled Zn dendrite growth and parasitic side-reactions, which changes local pH environment of electrolyte, compromises Coulombic efficiency (CE) and hinders their potential applicability.[4] Both the dendrite issue and parasitic side-reactions are associated with the active hydrated $Zn(OH)_6^{2+}$ ion and superabundant free water in common aqueous solution.[3c, 5] Apart from constructing surface blocking layers on the Zn metal anode, intensive investigations have been conducted to regulate the electrolyte by decreasing the number of free water and blocking water penetration to Zn surface. Representative examples include designing functional gel electrolyte,[6] constructing solid electrolyte interphase (SEI),[7] and introducing electrolyte additives.[8] However, the effectiveness for multivalent-metal electrolyte depends on an ideal coordination environment of

metal cations. Hence, strategies to effectively modulate the Zn^{2+} solvation structure are required to boost the stability performance of RZBs towards industrial applications.[3b]

The emergence of super-concentrated "water-in-salt" electrolytes is a significant step forward to high-efficient aqueous system.[9] In this electrolyte, the Lewis-acidic cations (Li^+, Zn^{2+}) coordinate with the oxygen donor in water or the Lewis-basic anion (F^-, Cl^-), forming metal-water-anion coordinated complexes. Furthermore, in the "water-in-salt" electrolyte system, almost all water molecules participate into the solvation sheath, resulting in substantially decrease and suppressed activity of free water. Unfortunately, the high price of electrolyte (e.g., $Li[N(SO_2CF_3)_2]$ or $Zn[(SO_3CF_3)_2]_2$), corrosiveness of Lewis acidic metal halides (e.g., $[Zn_xCl_{(2x+2)}]^{2-}$), and susceptibility to be oxidized (e.g., Cl^-) retrograde from Zn battery.[10] There is an urgent to find new safe, green and low-cost electrolyte contains unique Zn^{2+} coordination structure for RZBs. Deep eutectic solvent (DES) is formed through strong ion-dipole interaction among eutectic mixtures of Lewis or Brønsted acids and bases which contains a variety of anionic and/or cationic species.[11] It is essentially different from the aqueous with or without additives, concentrated or water/organic hybrid electrolytes. Even though the additives in an aqueous system and the organic co-solvent in hybrid systems may modulate the solvation structure, their chemical environments are totally different from that in a eutectic system. The type of zinc salt and ligand molecular (structure, size, molecular weight, dielectric constants, dipole moments) and their mole ratios will affect the physicochemical properties of the eutectic system. Furthermore, the hydrated Zn salts may lead to a lower melting point than the corresponding anhydrous salts because water molecules can decrease the lattice energy.[11d] For example, DES can be prepared by mixing zinc salts such as $ZnCl_2$, $Zn(CF_3SO_3)_2$, $Zn(ClO_4)_2 \cdot 6H_2O$ with ligands including choline chloride, ethylene glycol, urea, acetamide and N-methylacetamide.[11a, 12] While study on the charge transfer in an eutectic system is still immature, it has been proven that some additives like water, acetonitrile, fluoroethylene carbonate and ethylene glycol affect the viscosity and conductivity.[11a, 13] Notably, eutectic systems share their remarkable properties, e.g., low vapor pressure, moderate thermo-stability, wide electrochemical potential window and composition tunability.[14] Characterized by adjustable compositions and rich inter-molecular forces, very recently liquidus eutectic electrolyte has been leveraged toward highly stable Zn anode by suppressing the dendrites and side reactions.[10] However, the intrinsic high viscosity and low ionic conductivity of the reported systems have limited their potential in the aqueous batteries, in which hydrated protons

participate in the intercalation reaction to V- and Mn-based cathodes. It is hypothesized that an optimal degree of hydration in eutectic system will significantly impact the reversibility and stability of the aqueous Zn-based redox chemistry. Therefore, new kinds of eutectic electrolytes that possess facile synthesis, high conductivity, and cost-effectiveness properties, prepared through hydrated Zn salts, co-solvent additives and green ligand, will be a promising choice, which is reported in this paper.

Due to the large dielectric constants (47.39), dipole moments (4.44 D) and abundant sulfonyl group of MSM, it can serve as a strong Lewis base to coordinate with cations.[10b] Here in this work, a new HEE system composed of $Zn(ClO_4)_2 \cdot 6H_2O$, MSM and H_2O is deployed to enhance the reversibility of Zn redox reactions. This HEE system is induced by Zn^{2+}-O interactions between $Zn(ClO_4)_2$ and MSM, where the MSM (as the Lewis base) enters to the primary solvation shell of Zn^{2+} (as the Lewis acid) forming the Zn-(MSM)-(H_2O) solvation structure. Through systematic *in-situ* and *ex-situ* characterizations, we attest that this structure can deprive a consideration number of free water molecules and intensify the intermolecular interaction, leading effectively to dendrite-free Zn deposition and suppressed side reactions. The novel HEE system containing unique solvated structure of Zn^{2+} and inner eutectic network renders unprecedented reversibility of Zn redox reactions in the vanadium-based zinc batteries (~100% retention even after 1600 cycles at 1000 mA g^{-1}). This result provides a deep insight to the subtle correlation between electrolyte structure and RAZB performance.

2. Results and Discussion

2.1 New Eutectic Solvent Structure

It is known that a strong electrostatic interaction between Zn^{2+} and dipolar water molecules in the currently available aqueous Zn^{2+} electrolyte will result in active $[Zn(OH_2)_6]^{2+}$ ion.[10] Designing a deep eutectic solvent electrolyte using MSM organic ligand can tailor the hydrated Zn species and surrounding O-H bonds, and thus allows the formation of multi-Zn-cooperates instead of $[Zn(OH_2)_6]^{2+}$.[15] Herein, the miscibility limit of mixed MSM and $Zn(ClO_4)_2 \cdot 6H_2O$ in H_2O at varying molar ratios are shown in **Figure 1**a. It is found that a eutectic composition of $Zn(ClO_4)_2 \cdot 6H_2O$-MSM containing 1.2 mmol Zn salt and 3.6 mmol MSM (denoted as HEE-1.2) shows the highest miscibility without additional water, forming a stable, transparent, colorless liquid at room temperature, which can remain stable without phase separation up to four months. Notably, adding a small amount of

water into HEE-1.2 system would affect their physicochemical properties including ionic conductivity, viscosity, and thermal behavior. A suitable amount of water into the eutectic system can improve the conductivity and lower viscosity while retaining the original nanostructure. Nonetheless, there is an upper limit to that hydration, above which the water-water and Zn-water reactions will dominate the eutectic-water hybrid system so that the original system will be disturbed.[16]

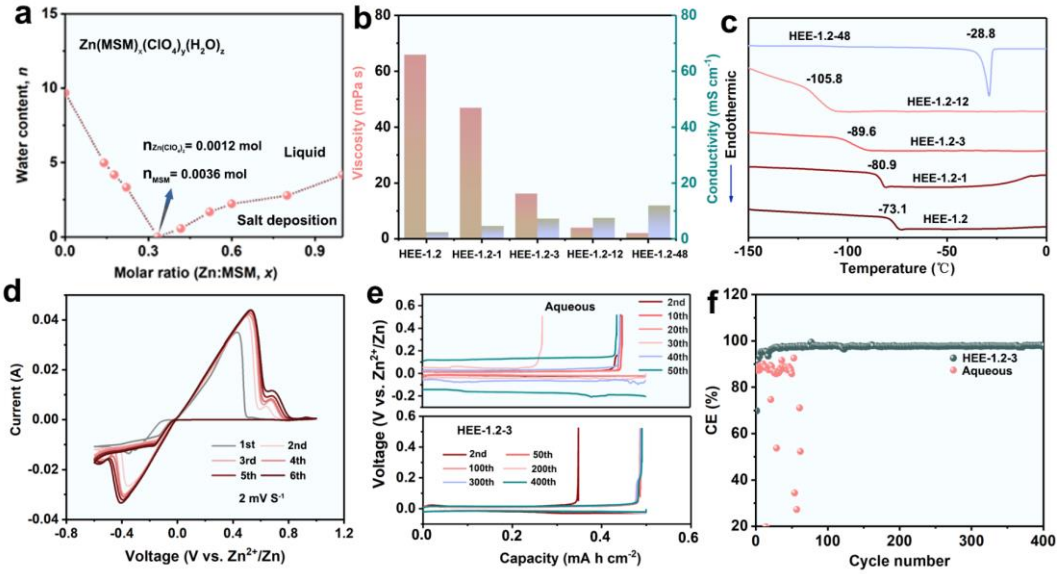

Figure 1. Physicochemical properties of eutectic electrolyte. a): Liquidus line of $Zn(ClO_4)_2$-MSM-H_2O mixtures. The data points on the liquidus line are determined through gradual addition of water to $Zn(ClO_4)_2$-MSM system at given values of *x*; b, c): Viscosity, conductivity and DSC data of $Zn(ClO_4)_2$-MSM-H_2O mixtures with different $Zn(ClO_4)_2$/MSM/H_2O ratios; d): Cyclic voltammetry curves of Zn plating/stripping using Cu as the working electrode, Zn as the reference and counter electrodes in HEE-1.2-3 electrolyte; e, f): Typical voltage profiles and corresponding CE of Zn plating/stripping in asymmetric Zn/Cu cells with aqueous and HEE-1.2-3 electrolytes.

The amount of water added to the HEE system is optimized by investigating its effect to the viscosity, ion conductivity, and thermodynamic stability of the formed eutectic electrolyte. Figure 1b reveals that viscosity reduces and ion conductivity increases with raising the H_2O ratio. The conductivity reaches 12.13 mS cm^{-1} for HEE-1.2-48 (viz., molar ratio of $Zn(ClO_4)_2 \cdot 6H_2O$, MSM and H_2O is 1.2: 3.6: 48), which is close to that in common aqueous electrolyte.[17] However, an opposite trend is observed to the rigid-to-plastic-crystal transition temperature. Differential scanning calorimetry (DSC) results (Figure 1c) show an endothermic peak at -28.8 ℃ for the HEE-1.2-48, which is much higher than that of HEE-1.2 (-73.1 ℃). It suggests that the HEE with high hydration

level would be close to an aqueous solution. As a result, the ternary MSM-$Zn(ClO_4)_2 \cdot 6H_2O$-H_2O mixture can form a liquid electrolyte at room-temperature while maintaining properties of eutectic system only at suitable compositions. In this study, the HEE-1.2-3 has been identified as the optimal electrolyte (molar ratio of $Zn(ClO_4)_2 \cdot 6H_2O$, MSM and H_2O is 1.2: 3.6: 3, conductivity: 7.4 mS cm^{-1}, viscosity: 16.3 mPa s, rigid-to-plastic-crystal transition temperature: -89.6 ℃, see detailed preparation process in Figure S1, Supporting Information).

Potentiondynamic behaviors of Zn metal in symmetric Zn//Zn and asymmetric Zn//Cu cells with aqueous and HEE-1.2-3 electrolytes are investigated. According to Figure 1d and Figure S2a (Supporting Information), the cyclic voltammetry (CV) curves demonstrate reversible electrochemical Zn plating/stripping in the HEE-1.2-3 media, but serious water decomposition occurs in the aqueous counterpart (Figure S2b, Supporting Information). To evaluate the rechargeability of Zn metal anode in the two-electrolyte system accurately, asymmetric Zn//Cu cells are tested with a practical areal capacity of 0.5 mA h cm^{-2} (current density: 0.5 mA cm^{-2}, final voltage: 0.5 V). The plating/stripping curves (Figure 1e) show that the cells using HEE-1.2-3 electrolyte display nearly the same voltage polarization (~ 20 mV) with that using aqueous electrolyte. However, the former presents much smoother voltage profiles and higher CE than the latter (Figure 1e, f). The CE of the HEE-based Zn//Cu reaches up to 97.4% after 50 cycles and maintains at about 98% during 400 cycles. In contrast, the CE of the cell fluctuates severely in the aqueous electrolyte which could be ascribed to the dendritic deposition, water evolution and side reactions.

2.2 Liquid Structure of Optimized HEE

Because of the intrinsic strong intermolecular interaction and absence of solvent molecules of eutectic electrolytes,[13] the physicochemical properties will be strongly affected by their composition, structure and dynamics feature. Raman spectroscopy is first undertaken to differentiate the liquid structure of HEE systems from that in aqueous media (**Figure 2**a and Figure S3a, Supporting Information). The aqueous electrolyte shows a broad Raman band consisting of several components in the range of 3100-3700 cm^{-1} (O-H stretching vibration mode), which is associated with strong hydrogen-bonding environments in water clusters.[18] This broad band remains pronounced in HEE-1.2-48, suggesting that water cluster will not participate in Zn^{2+} solvated shell. As the water contents gradually decrease, this peak vanishes and a new band at about 3500 cm^{-1} appears, which could be

attributed to water monomers with weak or no hydrogen bond.[14] This implies an evident decrease in the hydrogen-bond proportion in the HEE solution. Additionally, both the aqueous electrolyte and $Zn(ClO_4)_2 \cdot 6H_2O$ crystal display an obvious peak at 410 cm^{-1} assigned to the symmetric stretch of the octahedral $[Zn(H_2O)_6]^{2+}$.[10] However, it weakens in intensity and shifts to low frequency in HEE-1.2-3 system (Figure S4, Supporting Information), indicating decreased amount of $[Zn(H_2O)_6]^{2+}$ and a changed solvation structure of Zn^{2+}. Similar behavior can be inferred from Fourier transform infrared (FT-IR) spectra (Figure 2b and Figure S3b, Supporting Information). Both the characteristic "intermediate water" (3450 cm^{-1}) and "multimer water" (3550 cm^{-1}) related broad O-H stretching vibration can be observed in aqueous and HEE-1.2-48 electrolytes. Nonetheless, when the molar ratio of water is lowered, these two peaks decrease significantly in intensity, accompanied with redshift of the O-H bending vibration (~1620 cm^{-1}) (Figure 2c). This corroborates the implication that bulk water molecules nearly do not exist in HEE-1.2-3, instead they are isolated from each other forming the Zn-H_2O coordinated ionic phases.[14]

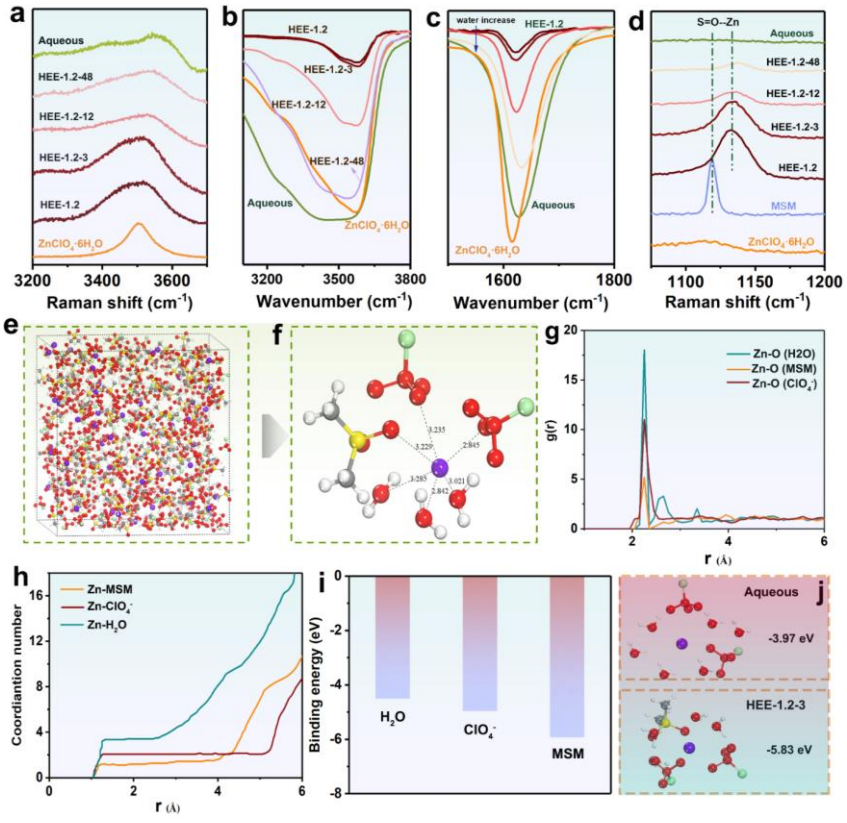

Figure 2. HEE structure analysis. a, d) Raman and b, c) FT-IR spectra of aqueous and HEE systems; e): 3D snapshot obtained by MD simulations and f) representative Zn^{2+}-solvation structure of HEE-1.2-3 solution; g, h): RDFs for Zn-O (H_2O), Zn-O (ClO_4^-) and Zn-O (MSM) and coordination number of Zn^{2+} collected from MD simulations in HEE-1.2-3 electrolyte; i): Binding energy of Zn^{2+} with

H_2O, MSM and ClO_4^- ion from DFT calculation; j): Total binding energy of representative Zn^{2+}-solvation structures in aqueous and HEE-1.2-3 electrolytes.

Raman spectra of the S=O stretching vibration (at 1133 cm^{-1}) is sensitive to the coordination environment of Zn^{2+} cations[19]. As shown in Figure 2d, the peak assigned to S=O bonding with Zn^{2+} decreases gradually in intensity with water content, suggesting the introduced water molecules has disturbed the original Zn-MSM coordination shell. Additionally, the ClO_4^- vibration in the FT-IR spectra splits to two peaks positioned at around 1088 and 1112 cm^{-1}, corresponding to Zn^{2+}-ClO_4^- ion pair and ClO_4^- free anion, respectively,[20] in both aqueous solution and $Zn(ClO_4)_2 \cdot 6H_2O$ crystal (Figure S5, Supporting Information). Obviously, the two peaks tend to merge from the bulk aqueous solution to $Zn(ClO_4)_2$-MSM-H_2O HEE-based system, implying a changed coordination environment of ClO_4^-.

Molecular dynamics (MD) simulations can provide more insights to the solvation structures of Zn^{2+} ions in aqueous and DES-1.2-3 systems. It is revealed that, Zn^{2+} remains well hydrated in its primary solvation sheath with sufficient free water available in aqueous solution, and many water clusters form a network through strong hydrogen bonds (Figure S6a, b, Supporting Information). In contrast, in the in HEE-1.2-3 electrolyte, one MSM molecule enters into the primary solvation sheath and replaces one water (Figure 2e, f). The corresponding radial distribution functions (RDFs) and coordination results are also obtained. A sharp peak centered at around 2 Å from Zn^{2+} could be ascribed to Zn-H_2O in primary solvation sheath in aqueous electrolyte model[21] (Figure S6c, Supporting Information). Similarly, both the peaks of Zn-H_2O and Zn-MSM appear in HEE-1.2-3 electrolyte model (Figure 2g), suggesting the existence of MSM in the primary solvation sheath. The average coordination number of Zn-H_2O and Zn-MSM in first hydration layer are 3.5 and 1.2 (Figure 2h), respectively, while it is 4.2 for Zn-H_2O in aqueous solution (Figure S6d, Supporting Information). All the above results imply a modulated solvation structure and a reduction of active water around Zn^{2+} in HEE-1.2-3 system. In addition, the modified solvation structure is also confirmed by density functional theory (DFT) calculations. A much higher binding energy of Zn^{2+}-MSM (-5.93 eV) than that of Zn^{2+}-H_2O (-4.51 eV) is revealed, indicating that MSM has a high tendency to join the solvation sheath of Zn^{2+} than that of H_2O (Figure 2i, j). Hence, a large amount of energy is required to break the Zn^{2+}-MSM bonds, which facilitates the homogeneous nucleation during the Zn plating.[17]

2.3 Stable Zn^{2+}/Zn Redox Reactions

The stability of Zn anode in both aqueous and HEE-1.2-3 electrolytes are evaluated by long-term galvanostatic cycling at different current densities. As illustrated in **Figure 3**a, despite of a larger polarization of Zn plating/stripping in HEE-1.2-3 electrolyte than that in aqueous solution due to its low ionic conductivity, the cell operates sustainably over 2000 hours without notable overpotential fluctuation, which is in sharp contrast to the erratic voltage response in aqueous electrolyte after only 60 hours. The cyclic stability was also tested to the HEE-1.2-3 at lower and higher current densities to check the Zn plating/stripping reversibility. First, an impressive stability with a cycling life over 2000 hours is also observed at 0.05 mA cm^{-2}. When cycled at a high current of 2 mA cm^{-2}, the HEE-1.2-3-based Zn//Zn cell still can maintain stable voltage response up to 400 hours without evident overpotential increase (Figure 3b).

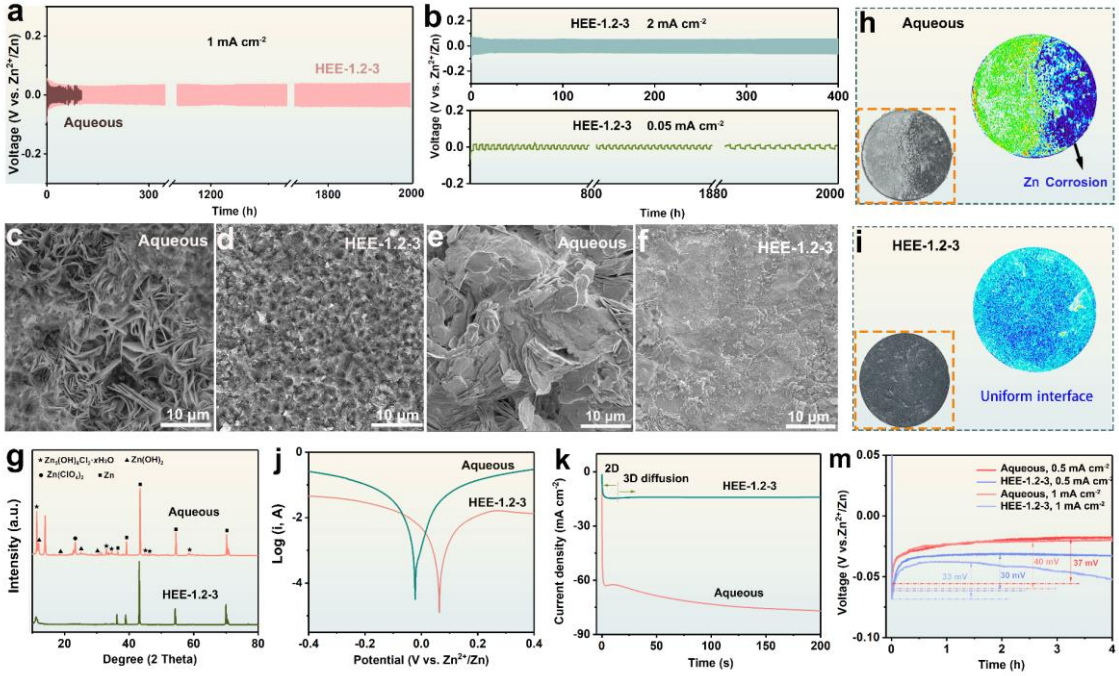

Figure 3. Zn plating/stripping and deposition behaviors in aqueous and HEE systems. a, b): Comparisons of voltage profiles in Zn//Zn symmetric cells; c, d) Typical SEM images of the deposited Zn metal on Cu substrate; e, f) SEM images of the Zn anode surface after 500 cycles in the Zn//Zn cell; g) XRD patterns and h, i) simulated images (Fiji App; University of Wisconsin, Madison, WI, USA) of Zn electrode after 500 cycles in the Zn//Zn cell. Insets are corresponding optical photos; j-m): Linear polarization curves showing the corrosion on Zn metal, Chronoamperograms of Zn metal at a -200 mV overpotential and typical voltage-time curves of Zn//Cu asymmetric cells in aqueous and HEE-1.2-3 electrolytes.

To shed light on the effect of solvation structure on the reversibility of Zn deposition, morphologies of platted Zn on Cu foil with deposition capacity of 5 mA h cm^{-2} are examined. SEM images show that irregular flake-like Zn growth with random alignment is observed in the aqueous electrolyte, while in the HEE-1.2-3 case, the deposited Zn is a compact and flat film (Figure 3c, d). This difference in deposition homogeneity is also verified from the optical images (insets in Figure S7, Supporting Information). Furthermore, the deposited Zn film in aqueous electrolyte is more than twice thicker than that in the HEE-1.2-3 electrolyte (see cross-sectional SEM images in Figure S7, Supporting Information). The resulting Zn dendrites growth may account for the low CE, degraded cycling performance and even the battery failure due to internal short circuits. In addition, the Zn//Zn half cells with aqueous and HEE after 500 stripping/plating cycles at 1 mA cm^{-2} were disassembled to explore the structural evolution of Zn electrode. The observation is quite similar to the Zn//Cu cell discovered above. The surface morphology of Zn metal in aqueous solution is uneven with characteristic Zn protrusions (Figure 3e). In addition, XRD patterns (Figure 3g) reveal large amounts of insulating byproducts including $Zn(OH)_2$, ZnO and $Zn_5(OH)_8Cl_2 \cdot xH_2O$. Furthermore, severe corrosion reactions in aqueous electrolyte are implied by the optical images and corresponding simulated images[22] (Figure 3h) which show an extremely rough surface of the Zn anode. In contrast, a quite uniform surface of Zn anode is observed in HEE-1.2-3 electrolyte (Figure 3f, i). It is observed that dendritic Zn growth and side reactions are aggravated with further increasing the current density to 3 mA cm^{-2}, which is the case for both aqueous and HEE-1.2-*x* ($48 > x > 3$) electrolytes (Figure S8, Supporting Information). However, a relatively flat and homogeneously Zn surface is maintained after cycling in the HEE-1.2-3 electrolyte. Therefore, it can be inferred that HEE-1.2-3 system has effectively suppressed Zn dendrites growth and various side reactions.

To further investigate the electrochemical behavior of Zn metal in different electrolytes, linear polarization experiment and chronoamperometry (CA) tests are conducted in symmetric cells. The lower current density and higher corrosion potential indicates improved thermodynamic stability of HEE-1.2-3 against Zn metal compared with aqueous system[23] (Figure 3j). The change of current under a constant overpotential is related with the evolution of nucleation process.[23] As for the routine aqueous case, the current keeps increasing during the total 200 s (Figure 3k), indicating a long and rampant 2D diffusion procedure in which the absorbed ions diffuse to energetically favored nucleation

sites. However, in order to minimize the surface energy and exposed area, Zn ions tend to aggregate and grow into dendrites. As for the case in HEE-1.2-3 media, Zn^{2+} ions diffuse in a dominating 3D surface because of the extra energy barrier of de-solvation caused by strong coordination interplay between Zn^{2+} and MSM. Thus, they are prone to be reduced and nucleate at the adsorbed sites, leading to a uniform and dense Zn deposition layer. Nucleation overpotential is also evaluated in Zn//Cu asymmetric cell (Figure 3m). The lower nucleation overpotentials both at 0.5 and 1 mA cm^{-2} in HEE-1.2-3 media than that in aqueous solution would contribute to more uniform nucleation in the former. Because of the significant reduced amount of free water clusters and weakened water-water hydrogen-bonding of HEE system, a limited water activity will expand the stable electrochemical window compared with that in aqueous solution. This expectation is confirmed from linear sweep voltammetry (LSV) curves (Figure S9, Supporting Information), which show an extension of potential window from 2.3 V in a typical aqueous solution to 2.7 V in the HEE-1.2-3.

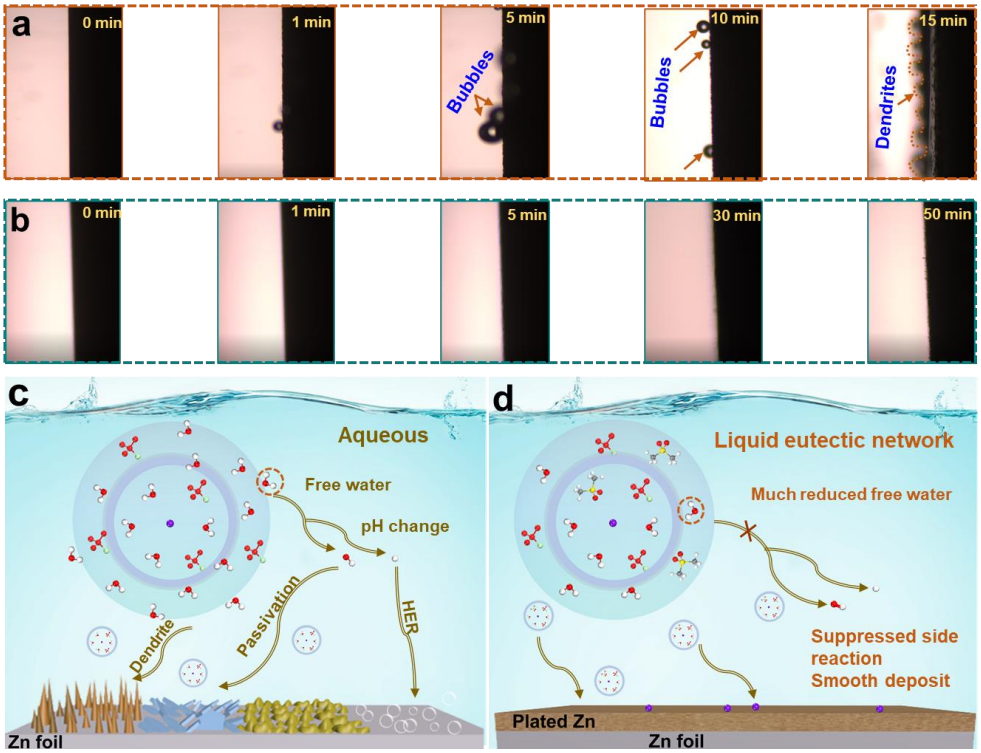

Figure 4. *In-situ* investigations of Zn deposition. Optical microscopy images of the Zn/electrolyte interfaces on Cu substrate in aqueous a) and HEE-1.2-3 b) electrolytes; c, d) Schematics of Zn^{2+}-solvated structures and Zn/electrolyte interface reactions in aqueous and HEE-1.2-3 systems, respectively.

To visualize the effect of HEE on suppressing dendrites growth and side reactions, the Zn plating pattern on Cu substrate at 5 mA is monitored with *in-situ* optical microscopy. Numerous protruding spots appear just after 1 min in aqueous electrolyte, and continuously grow into dendritic Zn after 15 min (**Figure 4**a). Meanwhile, gas bubbling (due to H_2 evolution reaction) resulting from high reactivity of free water is also detected. In the case of HEE-1.2-3-based cell, the Zn surface remains intact after 30 min without any gas evolution or Zn dendrite growth under the same condition (Figure 4b).

To summarize the above result, the Zn^{2+} solvation structures and interfacial reactions between Zn metal and electrolyte are depicted schematically in Figure 4c, d. Active free water and solvated water around Zn^{2+} are present in aqueous solution. As a result, electrochemical driven parasitic reactions including dendrite growth, passivation generation, hydrogen evolution and Zn metal corrosion occur spontaneously. In contrast, the number of free water molecules reduces significantly in HEE-1.2-3 electrolyte, and the coordination of MSM to Zn^{2+} reduces the affinity of water to Zn^{2+}. This solvation structure is beneficial in suppressing the side reactions and enabling smooth Zn deposition.

2.4 Demonstration of Vanadium-based Zn Batteries

To exemplify the feasibility of HEE in real RZBs, Zn//$NH_4V_4O_{10}$ (NVO) and Zn//CaV_4O_9 (CVO) cells are assembled. Morphology characterization of NVO and CVO is shown in Figure S10 (Supporting Information). For the Zn//NVO system, CV curves after the first cycle at 0.2 mV s^{-1} are almost overlapped (**Figure 5**a). The reversible redox reaction most likely involves a co-intercalation of Zn^{2+} and hydrated protons (H_3O^+) as reported in previous work.[24] As expectedly, HEE-1.2-3 electrolyte-based cells deliver high capacity-retentions of 91% (with respect to the highest value after initial activation) over 600 cycles at 500 mA g^{-1}, 92% after 100 cycles at 200 mA g^{-1} (Figure 5b and Figure S11a, Supporting Information), ~ 100% retention after 1600 cycles at 1000 mA g^{-1} (Figure 5d), and 76% retention after 3000 cycles at 3000 mA g^{-1} (Figure S11b, Supporting Information). The aqueous counterpart degrades drastically even at the low current density after only dozens of cycles (Figure 5b and Figure S11a, Supporting Information). Furthermore, Zn//NVO cells based on HEE-1.2-*x* (*x*= 0, 12, 48) or high-concentration 8 M $Zn(ClO_4)_2$ solution all display worse cycling performance (Figure S12 and S13, Supporting Information), verifying the influence of water concentration in the HEE system. In conclusion, the performances of both the Zn//Zn and Zn//NVO

cells in our study are competitive with many previous works of Zn batteries with different kinds of electrolytes (Table S1, Supporting Information).

Charging/discharging profiles after the 2nd and 100th cycles further confirm a higher overpotential in aqueous electrolyte than that in HEE-1.2-3 solution (Figure 5c), which is likely caused by severe side reactions including passivation formation on the Zn metal surface and Zn corrosion. Based on the optical and simulated images, and SEM images of the Zn metal anode stripped from Zn//NVO batteries after 100 cycles at 500 mA g^{-1} (Figure 5f-i and Figure S14 and 15), a corroded rough Zn surface with obvious dendrites is observed in the aqueous electrolyte. In contrast, in the HEE-1.2-3 electrolyte, the Zn surface remains flat and homogeneous. These results confirm the effectiveness of the modulated solvation structure and water-deficient system on suppressing dendrites and side reactions.

The potential of HEE for power-type RZBs is also evidenced by the attractive rate performance; with 25 times increase in current density, 50% of the initial capacity is maintained (Figure S16, Supporting Information). Aside from the laboratory-scale coin cells, pouch-type cells with a size of 4 × 4 cm^2 are also assembled, which deliver an average capacity of 250 mA h g^{-1} and a long-term cycling stability over 500 cycles at 500 mA g^{-1} (Figure 5e). As for the Zn//CVO batteries based on the HEE-1.2-3 electrolyte, after an electrochemical active process (~70 cycles at 500 mA g^{-1}), the capacity keeps nearly unchanged after 400 cycles (Figure S17, Supporting Information), demonstrating the compatibility of DES-1.2-3 electrolyte in the vanadium-based Zn cell.

3. Conclusion

We have developed a new type of hydrated eutectic electrolyte for Zn batteries. In this HEE system, Zn^{2+} cations are coordinated with MSM, H_2O and ClO_4^- forming the $Zn(MSM)_x(H_2O)_y(ClO_4)_z$ complexes. Systematic characterizations using Raman, FT-IR, MD and DFT calculations reveal that Zn coordinates with 3.5 H_2O, 2.1 ClO_4^- and 1.2 MSM in the primary shell in optimized HEE-1.2-3 electrolyte system. Because of reduced amount of free and solvated water around Zn^{2+} in the HEE-1.2-3 solution than that in common aqueous solution, the Zn dendrite growth, water reduction and interface side reactions are significantly suppressed. Accordingly, the electrochemical stability window has also been expanded. Galvanostatic cycling of Zn//Zn symmetrical cells demonstrates an ultrastable Zn platting/stripping process, in which the homogeneous Zn deposition without gas

evolution is proved using *in-situ* optical microscopy. In the vanadium-based Zn cell, this subtle designed HEE system enables the vanadium-based aqueous Zn metal batteries with high capacity and cycling performance. Overall, our study on this new hydrated eutectic electrolyte offers new insights into green electrolyte systems to boost the performance of the promising Zn based batteries.

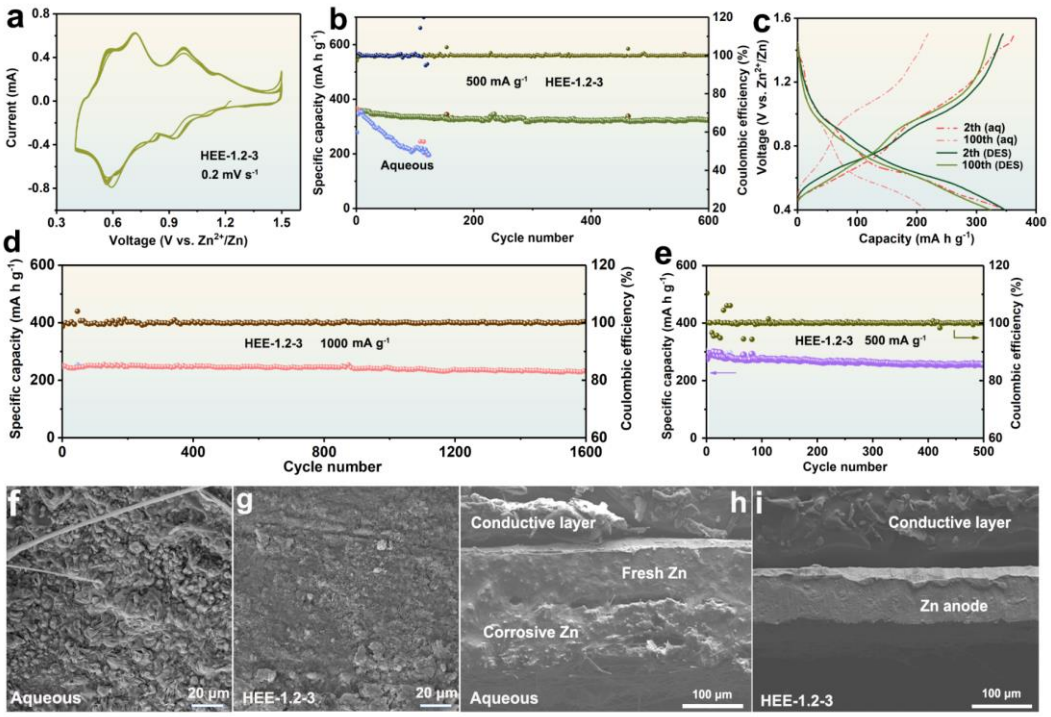

Figure 5. Zn//NVO battery in aqueous and HEE-1.2-3 electrolytes. a): CV curves at 0.2 mV s^{-1}; b, d) Cycling performance of at two current densities of 0.5 and 1 A g^{-1}; c) Charge/discharge curves at the different cycles; e) Cycling performance of a pouch cell with a cathode mass loading of 1.7 mg cm^{-2}; f, g) Top-view and h,j) cross-sectional SEM images of the Zn anode after 100 cycles at 500 mA g^{-1}.

Supporting Information

Supporting Information is available from the Wiley Online Library or from the author.

Acknowledgements

This work was supported by the National Natural Science Foundation of China (Grant Nos. 51972346, 51932011), the Hunan Natural Science Fund for Distinguished Young Scholar (2021JJ1006), the Program of Youth Talent Support for Hunan Province (2020RC3011), the Innovation-Driven Project

of Central South University (No. 2020CX024), and the Fundamental Research Funds for the Central Universities of Central South University (No. 202321024). H.J.F acknowledges the financial support from Ministry of Education by Tier 1 grant (RG85/20).

Conflict of Interest

The authors declare no conflict of interest.

Keywords

Hydrated eutectic solvent electrolyte, Zn^{2+} solvation structure, Zn dendrites, Ligand-oriented solvation shell, Aqueous zinc battery

References

[1] a) M. Han, L. Qin, Z. Liu, L. Zhang, X. Li, B. Lu, J. Huang, S. Liang, J. Zhou, *Mater. Today Energy* 2021, *20*, 100626; b) M. Song, H. Tan, D. Chao, H. J. Fan, *Adv. Funct. Mater*. 2018, *28*, 1802564; c) G. Fang, J. Zhou, A. Pan, S. Liang, *ACS Energy Lett*. 2018, *3*, 2480-2501; d) S. Yang, M. Zhang, X. Wu, X. Wu, F. Zeng, Y. Li, S. Duan, D. Fan, Y. Yang, X. Wu, *J. Electroanal. Chem*. **2019**, *832*, 69-74.

[2] a) W. Sun, F. Wang, S. Hou, C. Yang, X. Fan, Z. Ma, T. Gao, F. Han, R. Hu, M. Zhu, C. Wang, *J. Am. Chem. Soc.* **2017**, *139*, 9775-9778; b) D. Kundu, B. D. Adams, V. Duffort, S. H. Vajargah, L. F. Nazar, *Nat. Energy* **2016**, *1*, 16119; c) M. Yan, P. He, Y. Chen, S. Wang, Q. Wei, K. Zhao, X. Xu, Q. An, Y. Shuang, Y. Shao, K. T. Mueller, L. Mai, J. Liu, J. Yang, *Adv. Mater.* **2018**, *30*, 1703725; d) X. Guo, J. Zhou, C. Bai, X. Li, G. Fang, S. Liang, *Mater. Today Energy* **2020**, *16*, 100396.

[3] a) J. Zheng, Q. Zhao, T. Tang, J. Yin, C. D. Quilty, G. D. Renderos, X. Liu, Y. Deng, L. Wang, D. C. Bock, C. Jaye, D. Zhang, E. S. Takeuchi, K. J. Takeuchi, A. C. Marschilok, L. A. Archer, *Science*, **2019**, *366*, 645–648 ; b) Q. Zhang, J. Luan, Y. Tang, X. Ji, H. Wang, *Angew. Chem. Int. Ed.* **2020**, *59*, 13180-13191; c) J. Hao, L. Yuan, C. Ye, D. Chao, K. Davey, Z. Guo, S. Z. Qiao, *Angew. Chem. Int. Ed.* **2021**, *60*, 7366-7375.

[4] a) L. Ma, M. A. Schroeder, O. Borodin, T. P. Pollard, M. S. Ding, C. Wang, K. Xu, *Nat. Energy* **2020**, *5*, 743-749; b) X. Xie, S. Liang, J. Gao, S. Guo, J. Guo, C. Wang, G. Xu, X. Wu, G. Chen,

J. Zhou, *Energy Environ. Sci.* **2020**, *13*, 503-510.

[5] M. R. Lukatskaya, J. I. Feldblyum, D. G. Mackanic, F. Lissel, D. L. Michels, Y. Cui, Z. Bao, *Energy Environ. Sci.* **2018**, *11*, 2876-2883.

[6] a) Y. Tang, C. Liu, H. Zhu, X. Xie, J. Gao, C. Deng, M. Han, S. Liang, J. Zhou, *Energy Storage Mater.* **2020**, *27*, 109-116; b) J. Gao, X. Xie, S. Liang, B. Lu, J. Zhou, *Nano-Micro Lett.* **2021**, *13*, 69.

[7] a) D. Li, L. Cao, T. Deng, S. Liu, C. Wang, *Angew. Chem. Int. Ed.* **2021**, *60*, 13035-13041; b) H. Qiu, X. Du, J. Zhao, Y. Wang, J. Ju, Z. Chen, Z. Hu, D. Yan, X. Zhou, G. Cui, *Nat. Commun.* **2019**, *10*, 5374.

[8] a) W. Xu, K. Zhao, W. Huo, Y. Wang, G. Yao, X. Gu, H. Cheng, L. Mai, C. Hu, X. Wang, *Nano Energy* **2019**, *62*, 275-281; b) Y. Dong, L. Miao, G. Ma, S. Di, Y. Wang, L. Wang, J. Xu, N. Zhang, *Chem. Sci.* **2021**, *12*, 5843-5852; c) P. Wang, X. Xie, Z. Xing, X. Chen, G. Fang, B. Lu, J. Zhou, S. Liang, H. J. Fan, *Adv. Energy Mater.* **2021**, *11,* 2101158.

[9] a) L. Suo, O. Borodin, T. Gao, M. Olguin, J. Ho, X. Fan, C. Luo, C. Wang, K. Xu, *Science* **2015**, *350*, 938-943; b) C. Zhang, J. Holoubek, X. Wu, A. Daniyar, L. Zhu, C. Chen, D. P. Leonard, I. A. Rodríguez-Pérez, J. X. Jiang, C. Fang, X. Ji, *Chem. Commun.* **2018**, *54*, 14097.

[10] a) W. Yang, X. Du, J. Zhao, Z. Chen, J. Li, J. Xie, Y. Zhang, Z. Cui, Q. Kong, Z. Zhao, C. Wang, Q. Zhang, G. Cui, *Joule* **2020**, *4*, 1557-1574; b) P. Jiang, L. Chen, H. Shao, S. Huang, Q. Wang, Y. Su, X. Yan, X. Liang, J. Zhang, J. Feng, Z. Liu, *ACS Energy Lett*. **2019**, *4*, 1419-1426.

[11] a) C. Zhang, L. Zhang, G. Yu, *Acc. Chem. Res.* **2020**, *53*, 1648-1659; b) C. Zhang, L. Zhang, Y. Ding, X. Guo, G. Yu, *ACS Energy Lett.* **2018**, *3*, 2875-2883; c) J. Song, Y. Si, W. Guo, D. Wang, Y. Fu, *Angew. Chem. Int. Ed.* **2021**, *60*, 9881-9885; d) E. L. Smith, A. P. Abbott, K. S. Ryder, *Chem. Rev.* **2014**, *114*, 11060-11082.

[12] W. Kao-ian, R. Pornprasertsuk, P. Thamyongkit, T. Maiyalagan, S. Kheawhom, *J. Electrochem. Soc.* **2019**, *166*, A1063-A1069;

[13] J. Wu, Q. Liang, X. Yu, Q. F. Lü, L. Ma, X. Qin, G. Chen, B. Li, *Adv. Funct. Mater.* **2021,** 2011102.

[14] P. Jiang, L. Chen, H. Shao, S. Huang, Q. Wang, Y. Su, X. Yan, X. Liang, J. Zhang, J. Feng, Z. Liu, *ACS Energy Lett*. **2019**, *4*, 1419-1426.

[15] Y. Yamada, K. Usui, K. Sodeyama, S. Ko, Y. Tateyama, A. Yamada, *Nat. Energy* **2016**, *1*, 1-9.

[16] O. S. Hammond, D. T. Bowron, K. J. Edler, *Angew. Chem. Int. Ed.* **2017**, *56*, 9782-9785.

[17] R. Qin, Y. Wang, M. Zhang, Y. Wang, S. Ding, A. Song, H. Yi, L. Yang, Y. Song, Y. Cui, J. Liu, Z. Wang, S. Li, Q. Zhao, F. Pan, *Nano Energy* **2021**, *80,* 105478.

[18] a) J. Xie, Z. Liang, Y. C. Lu, *Nat. Mater.* **2020**, *19*, 1006-1011; b) Q. Nian, J. Wang, S. Liu, T. Sun, S. Zheng, Y. Zhang, Z. Tao, J. Chen, *Angew. Chem. Int. Ed.* **2019**, *58*, 16994-16999.

[19] L. Legrand, A. Tranchant, R. Messina, F. Romain, A. Lautie, *Inorg. Chem.* **1995**, *35*, 1310-1312.

[20] a) N. S. Venkata Narayanan, B. V. Ashokraj, S. Sampath, *J. Colloid Interface Sci.* **2010**, *342*, 505-512; b) N. S. V. Narayanan, B. V. Ashokraj, S. Sampathz, *J. Electrochem. Soc.* **2009**, *156*, A863-A872.

[21] P. Sun, L. Ma, W. Zhou, M. Qiu, Z. Wang, D. Chao, W. Mai, *Angew. Chem. Int. Ed.* **2021**, *60*, 18247-18255.

[22] J. Schindelin, I. Arganda-Carreras, E. Frise, V. Kaynig, M. Longair, T. Pietzsch, S. Preibisch, C. Rueden, S. Saalfeld, B. Schmid, J. Y. Tinevez, D. J. White, V. Hartenstein, K. Eliceiri, P. Tomancak, A. Cardona, *Nat. Methods* **2012**, *9*, 676-682.

[23] Z. Zhao, J. Zhao, Z. Hu, J. Li, J. Li, Y. Zhang, C. Wang, G. Cui, *Energy Environ. Sci.* **2019**, *12*, 1938-1949.

[24] a) B. Tang, J. Zhou, G. Fang, F. Liu, C. Zhu, C. Wang, A. Pan, S. Liang, *J. Mater. Chem. A* **2019**, *7*, 940-945; b) F. Wan, Z. Niu, *Angew. Chem. Int. Ed.* **2019**, *58*, 16358-16367.